OPEN ACCESS
IOP Publishing
Nanotechnology 25 (2014) 455603 (10pp)
Nanotechnology
doi:10.1088/0957-4484/25/45/455603

InAs migration on released, wrinkled InGaAs membranes used as virtual substrate

S Filipe Covre da Silva[1,2], E M Lanzoni[1], V de Araujo Barboza[1], A Malachias[3], S Kiravittaya[4] and Ch Deneke[1]

[1] Laboratório Nacional de Nanotecnologia (LNNano/CNPEM), Rua Giuseppe Máximo Scolfaro 10000, 13083-100, Campinas, Brazil
[2] Departamento de Física, Universidade Federal de Viçosa, 36570-000-Viçosa, MG, Brazil
[3] Departamento de Física, Universidade Federal de Minas Gerais, 30123-970-Belo Horizonte, MG, Brazil
[4] Department of Electrical and Computer Engineering, Faculty of Engineering, Naresuan University, Phitsanulok 65000, Thailand

E-mail: christoph.deneke@lnnano.cnpem.br

Received 8 July 2014, revised 18 August 2014
Accepted for publication 15 September 2014
Published 24 October 2014

Abstract

Partly released, relaxed and wrinkled InGaAs membranes are used as virtual substrates for overgrowth with InAs. Such samples exhibit different lattice parameters for the unreleased epitaxial parts, the released flat, back-bond areas and the released wrinkled areas. A large InAs migration towards the released membrane is observed with a material accumulation on top of the freestanding wrinkles during overgrowth. A semi-quantitative analysis of the misfit strain shows that the material migrates to the areas of the sample with the lowest misfit strain, which we consider as the areas of the lowest chemical potential of the surface. Material migration is also observed for the edge-supported, freestanding InGaAs membranes found on these samples. Our results show that the released, wrinkled nanomembranes offer a growth template for InAs deposition that fundamentally changes the migration behavior of the deposited material on the growth surface.

Keywords: freestanding membranes, patterned substrate, InAs growth

(Some figures may appear in colour only in the online journal)

Introduction

The growth of InAs on GaAs (001) substrates is one of the oldest, and most explored hetero-epitaxy systems [1–4]. Self-assembled InAs islands are widely explored in optical and opto-electronic devices as well as studied as one of the model systems of hetero-epitaxy [5–8]. Thereby, besides fundamental growth studies, the site control of such structures is of great interest using pattern substrates [5, 9–14]. Recently, a new class of patterned substrates has been introduced for controlling the formation of self-assembled nanostructures during growth [15–18]. The most common approach is the use of some kind of lithographical patterning, i.e. defining holes to modulate the chemical potential of the surface [19]. This alternative approach uses freestanding nanomembranes [20–24] with a thickness in the range of the lateral and vertical dimensions of the self-assembled nanostructure as compliant substrates [25, 26] for material deposition. Partly released membranes were shown to form three-dimensional (3D) wrinkle networks on top of the flat substrate due to strain relaxation [27–30]. Experimental results demonstrate that the growth on top of freestanding nanomembranes results in strain-mediated effects such as preferred nucleation on the membrane and ordering of the formed structures [16, 18, 31, 32]. Until now, the group IV elements [16, 18] or InAs on Silicon-on-Insulator [15] were explored with this technique, e.g. to realize high quality SiGe quantum cascade lasers on top of a relaxed SiGe membranes [33].

0957-4484/14/455603+10$33.00

สำเนาถูกต้อง
Sumit Kiravittaya
สุวิทย์ กิระวิทยา

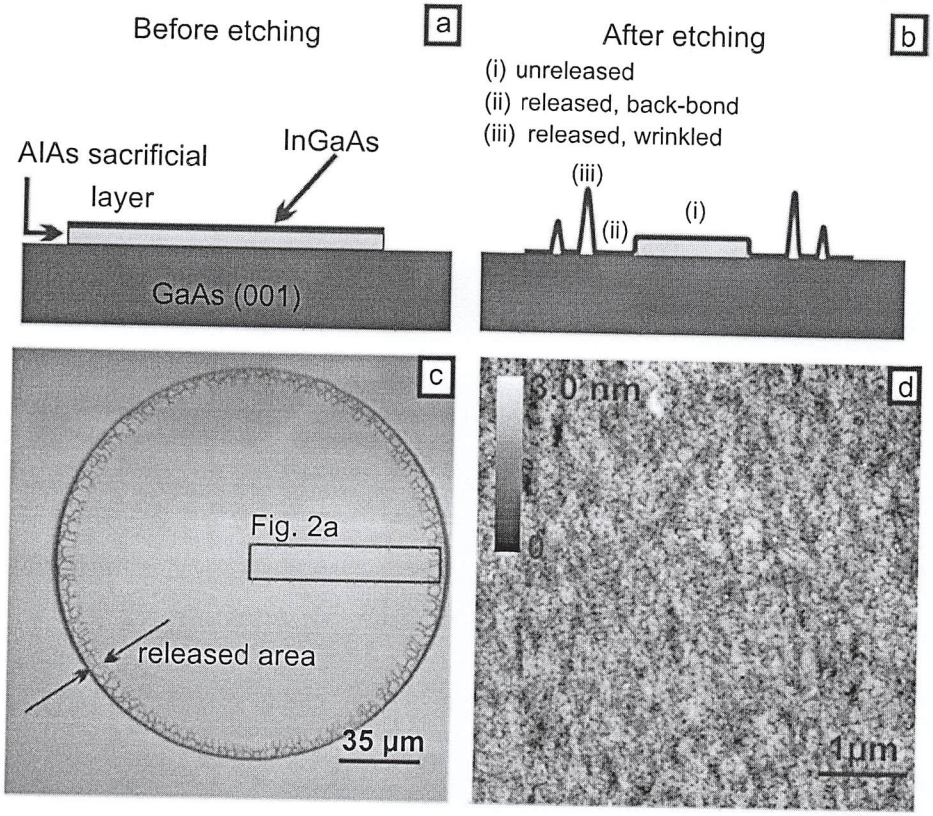

Figure 1. Schematic illustration of the sample fabrication: (a) processed sample before membrane release and (b) after partial underetching with wrinkle formation at the mesa border regions. (c) Light microscopy image of the sample showing the wrinkles that form after the InGaAs layer is released (The box marks the size of the AFM scan in figure 2(a)). (d) AFM image of the unreleased part of the sample after hydrogen cleaning.

Here, we extend this approach to partly released InGaAs membranes on which InAs is deposited using molecular beam epitaxy (MBE). The partly released membrane used as substrate exhibits a wrinkle network, where the strain in the InGaAs layer relaxes and freestanding 3D curved structures have formed [27]. Such samples exhibit three distinguished parts (see figure 1(b)): (i) unreleased areas, where the epitaxial layer is still connected to the unetched sacrificial layer; (ii) released, bond-back parts, where the InGaAs layer relaxes and bonds to the underlying GaAs (001) substrate; and (iii) freestanding wrinkles, where the InGaAs layer forms 3D structures. The formation of self-assembled InAs nanostructures is studied on the substrates that exhibit three different lattice parameters in close lateral proximity [29]. Using atomic force microscopy (AFM), the material migration of the InAs is studied. We find that the InAs migrates almost completely to the released, wrinkled areas of the substrate, where the InAs accumulates on top of the wrinkles of the released membrane. The migration occurs over distances as large as 60 μm during growth, leaving a flatted, island-free surface in the areas behind, where the membrane is not released. A semi-quantitative analysis of the misfit strain, which we consider the main contribution to the chemical potential changes of the surface, reveals that the curvature of the wrinkled membranes results into a minimal misfit strain for the deposited material. Therefore, it is the most attractive position for the lattice mismatched InAs and acts as sink for InAs migrating over the surface. The large observed migration length is in agreement with calculations [34] predicting an enlarged diffusion coefficient for compressively strained InGaAs surfaces. Finally, we observe InAs accumulation preferably on top of free-standing InGaAs membranes. Reasons for this can either be an initial surface curvature due to the strain relaxation of the edge-supported membrane and/or a strain transfer of the self-assembled nanostructures to the compliant substrate. The latter scenario is supported by grazing-incidence x-ray diffraction measurements, which evidence the existence of regions where the deposited material exhibits intermediate lattice parameter, between the InAs and GaAs values.

Experimental details

The fabrication process for our samples is illustrated in figures 1(a) and (b). We use a commercially available 20 nm AlAs/5 nm $In_{0.33}Ga_{0.67}As$ heterostructures (EpiNova) grown on top of a GaAs (001) substrate for our experiments. The

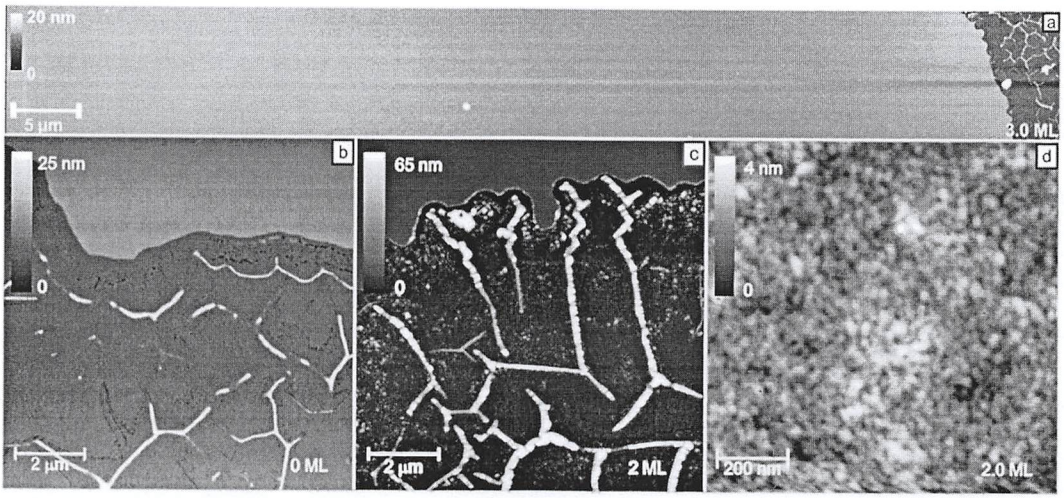

Figure 2. (a) An AFM $80 \times 10\,\mu$m overview image illustrating the large migration length of the InAs from the unreleased areas to the released, wrinkled regions. (b) $10 \times 10\,\mu$m AFM image of sample with 0 ML InAs deposited. (c) $10 \times 10\,\mu$m AFM image showing the frontier region between released and unreleased parts of a 2 ML sample. (d) AFM image of the unreleased area of the membrane surface.

heterostructure is patterned with a photolithography process defining circular 150 μm wide mesas. Trenches are etched into the heterostructure and the underlying substrate using a H_3PO_4:H_2O_2:H_2O (1:2:10) solution (figure 1(a)). To remove the photoresists after trench etching and to obtain an epi-ready sample surface, the photoresist is striped in a hot dimethylsulfoxide followed by a cascade cleaning in three times acetone for 30 s, 20 s, 10 s and a finally dip into in isopropyl alcohol, respectively. For complete resist removal, the sample is exposed for 10 min to an oxygen plasma inside a barrel reactor (Barrel Asher Plasma Technology SE80). In the next chemical-cleaning step, the sample is put into H_2SO_4 and etched for 10 min in an ultrasonic bath. Afterwards, it is cleaned in SemiconClean23 (Furuuchi Kagaku K.K., Japan) for 2 min and rinsed for 10 min in a water flow bath. To obtain the partly released layers, we selectively remove the parts of the AlAs layer using a diluted HF solution (figure 1(b)). In figure 1(b), we marked the three distinguished regimes of the sample (i) unreleased parts; (ii) released, backbond areas; and (iii) released, wrinkled areas. Figure 1(c) depicts a light microscopy image of the defined round mesas with the released areas visible on the border of the mesa. The image shows that the released film starts to wrinkle inside areas of 5 to 10 μm wide (depending of the HF concentration and etching time). The box marks the size of the AFM scan in figure 2(a) for later comparison.

To overgrow our samples, we use the MBE facility of the LNNano (CNPEM, Brazil). Inside the MBE system, the sample was heated to 350 °C and a hydrogen cleaning was used to remove the native top oxide layer as well as carbon contaminants without damaging the thin, released membranes [35]. Figure 1(d) shows an AFM image obtained after the cleaning process. The image indicates that our surface stays intact and flat after the cleaning process and can be used for epitaxial growth afterwards. Furthermore, *in situ* reflective high-energy electron diffraction (RHEED) showed a streaky pattern after the cleaning process demonstrating a complete removal of the native oxide layer before growth.

For the overgrowth, the samples are introduced to the main chamber of the MBE. Different amounts of InAs (in monolayers (ML) of InAs) from 0 ML to 3 ML were deposited with a growth rate of 0.022 ML sec^{-1} a substrate temperature of 490 °C ± 10 °C. For the first sample series, a post-growth annealing step of 5 min followed by a rapid quenching of the substrate temperature was carried out. For a second growth series, the sample was quenched immediately after material deposition by turning off the heater power supply. Due to the construction of the MBE system, we achieve cooling rates of ca. 20 °C min^{-1} with this method. The growth was continuously monitored by RHEEED through the whole growth process.

A reference sample was prepared in which the final etching step to release the membrane was omitted. This resulted in a surface that exhibits the mesa structures depicted in figure 1(a), but no wrinkle network is formed. The sample has undergone the same growth procedure outlined above with 2 ML of InAs deposited.

Two AFM systems (NX10 Park System and Digital Instruments Nanoscope IIIa) were used to study the sample topography before and after the growth. Images were post-processed using the SPM software Gwyddion.

Gracing incidence x-ray diffraction (GIXRD) was carried out using the XRD2 beamline (LNLS, Brazil) using a fixed energy of 9.5 keV. The beam size (defined by slits) on the sample position was of 0.7 mm × 0.5 mm. The incident angle was fixed to 0.2° and a Pilatus 100 K detector was used, integrating an exit angle of 2°. Using such an incident angle below the critical angle of total external reflection, a penetration depth is of the order of 5 nm is expected. In the conditions above, the footprint of the beam spreads over the whole sample along the incident beam path. The central part of such footprint is then selected for diffraction in the vertical

plane by scattering slits and detector slits, both closed to 2 mm. Scans near the in-plane GaAs (220) reflection were investigated, in order to deduce the lattice parameters of the partly released, wrinkled sample with 2 ML InAs deposited onto it.

Results and discussion

Figure 2(a) shows an overview AFM image of $80 \times 10\,\mu$m corresponding to the area marked in figure 1(c) of the released and unreleased areas of a patterned mesa for a sample with an InAs deposition of 3 ML. The released area can be identified by its typical wrinkled structure, as seen on the right side of the image. The unreleased part—major flat area depicted in figure 2(a)—shows one growth defect in the middle, resulting from an etching pinhole. This pinhole leads to a small free-standing etch-supported InGaAs membrane attracting material—an effect discussed in more detail later. The released, back-bond parts show a clear material accumulation along the wrinkled areas and some material accumulation on the flat parts of the membrane. Such observations in the overview AFM image indicate a strong material migration during growth, from the unreleased, flat areas of our sample, towards the released, wrinkled regions.

To demonstrate the InAs migration better, figure 2(b) shows a sample with 0 ML deposition of InAs—hence the sample had undergone the growth process without opening the In shutter. In figure 2(b), the wrinkles, as well as the unreleased parts of the sample, can clearly be distinguished by the height step in the middle of the image. The AFM shows that the wrinkled surface stays intact. Furthermore, no indium accumulation is visible neither on the frontier between the unreleased and released parts, nor on top of the wrinkles. This demonstrates that the indium does not segregate out of the membrane (or the unreleased parts of the InGaAs epilayer) and the observed InAs accumulations in figure 2(a) are arising from the deposited material.

For comparison, the released wrinkled area of a sample with 2 ML of InAs deposited is depicted in figure 2(c). Again, the released area can be identified by the wrinkled membrane structures in the AFM topography image. Furthermore, the InAs accumulation on top of the wrinkles and on the frontier between the released and unreleased areas is visible. The deposited material forms chains of island-like structures on top of the wrinkles as well as on the flat areas, indicating that the Stranski–Krastanov growth mode for InAs remains intact.

Our interpretation that most of the deposited material migrates to the released, wrinkled sample regions is further supported by the AFM scan depicted in figure 2(d) showing the topography of the unreleased parts of the sample. The topographic image of the surface exhibits an overall height scale of 4 nm, which is comparable with the height scale of 3 nm of the initial growth surface seen in figure 1(d). Comparing the two surface topographies of figures 2(d) and 1(d) suggests some flattening of the initial growth surface but no major changes in the morphology.

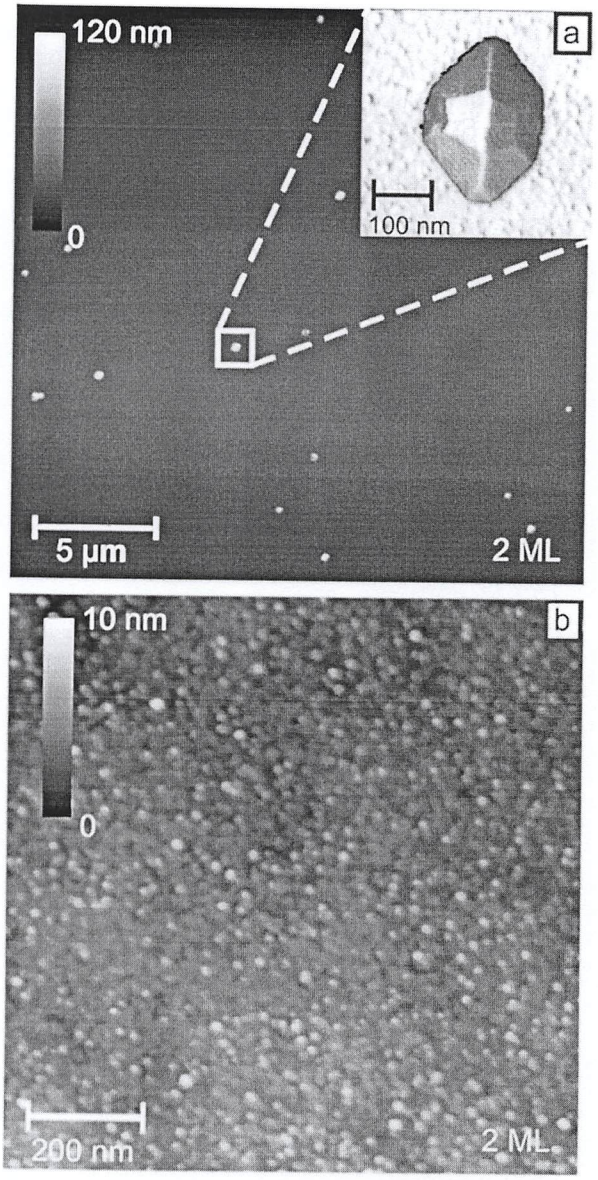

Figure 3. (a) Overview $20 \times 20\,\mu$m AFM image of a reference sample with 2 ML InAs deposited. Due to the 5 min post-annealing, large well faceted (see inset) InAs clusters developed. (b) $1 \times 1\,\mu$m AFM image of the reference sample surface. A clear formation of high density InAs islands is observed.

As a reference, we show in figures 3(a) and (b) AFM images of patterned samples without carrying out the final release of the membranes. The $20 \times 20\,\mu$m overview image (figure 3(a)) indicates the formation of large InAs clusters on the flat parts of the surface. The inset in figure 3(a) shows the surface slope of such a large InAs structure. In the surface slope plot, clear facets of the formed cluster can be identified as (137), (101) and (111) assigned by comparison with Ref. [36]. The height of our structures of 120 nm indicates that these islands are not longer coherent to the substrate but should be dislocated.

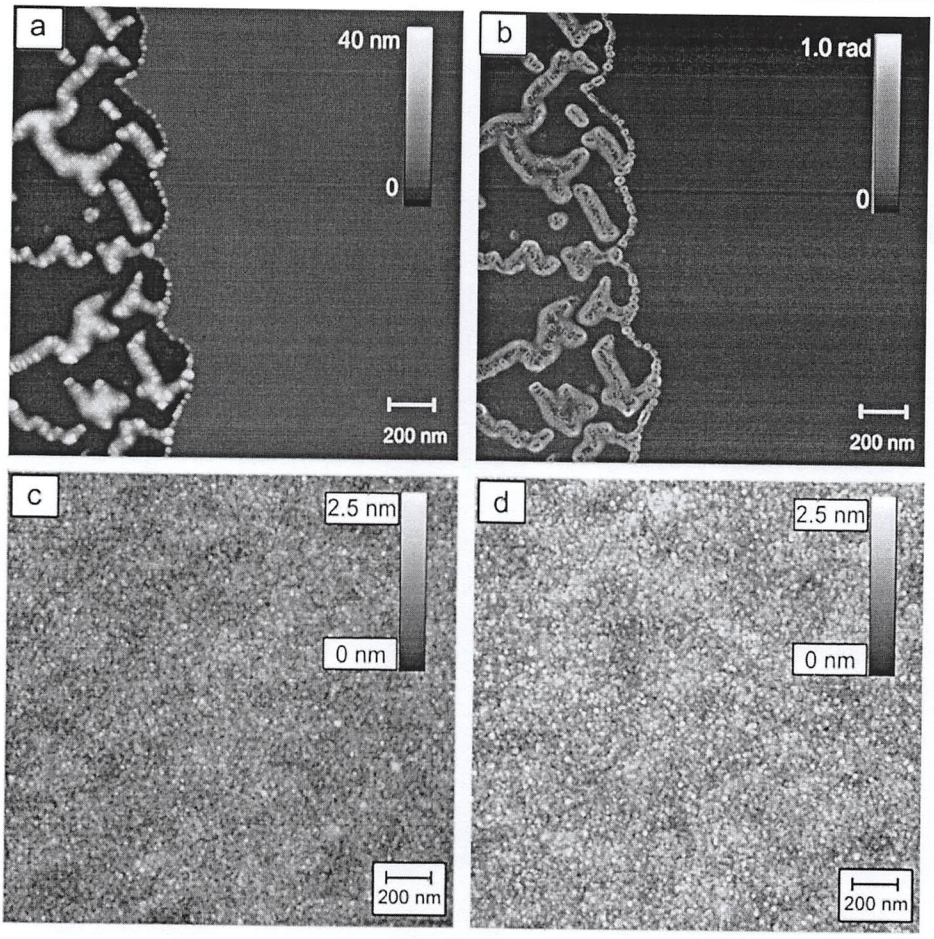

Figure 4. (a) AFM topography of the border between a relaxed, back-bond part and the unreleased areas of a quenched sample with 2 ML InAs deposited. (b) Slope plot to identify the island structures in image (a). (c) Flat area next to a released part of a quenched InAs sample. Only a small number of small InAs islands can be observed. (d) Flat area 12 μm away from the released areas [height scale adapted to fit figure (c)]. A larger amount of InAs islands indicate that part of the diffusion process occurs during the post-annealing, but the major material migration already takes place during InAs growth.

A 1×1 μm AFM image (figure 3(b)) of the area between these large structures reveals the existence of a high density of small InAs islands on the surface. These small islands are expected for this kind of sample, as the critical thickness for dot formation on GaAs (001) for InAs is ca. 1.8 ML. As the unreleased top InGaAs of the overgrown heterostructure still exhibits the lattice parameter of GaAs, the critical thickness for our samples should be below this value. Therefore, we were surprised to observe no formation of InAs islands on our patterned samples that had released areas (see e.g. figure 2(d)). This observation was consistent for all deposited InAs amounts ranging from 0.5 ML to 3 ML and supports our interpretation that all the material migrates to the released parts of the samples.

To investigate whether the material migration happens during growth as assumed for the depletion regions observed in patterned substrates [9] or mainly in our 5 min post-growth annealing, a second series of samples was grown. For this series, the heater was switched off immediately after InAs deposition to quench the sample and suppress any post-growth annealing and material migration.

Figure 4(a) depicts the topographic AFM image of a sample with 2 ML InAs deposited and quenched after growth at the border between the unreleased and the released, wrinkled areas. The etching frontier is clearly identifiable by the height step in the middle of the image. Furthermore, we again observe a great material accumulation on top of the wrinkled structure as well as at the border between the released and the unreleased areas of the sample. The island formation happened nearly exclusively either on top of the border or on top of the wrinkles. To illustrate this behavior more clearly, figure 4(b) shows the slope plot of the surface. As the back-bonded parts as well as the unreleased parts are basically flat, they appear black in this presentation of the surface. The InAs islands are clearly identifiable by their shape in the slope plot. Furthermore, the slope plot clearly shows that island formation exclusively occurs on sample position with a high slope —either at the height step between the released and

unreleased parts or on top of the wrinkles inside the released areas. Very few structures are observed on top of the flat relaxed, back-bond areas of the sample. This observation, in conjunction the larger volume (estimated) of InAs on top of the wrinkled area, supports our conclusion that the material migrates from the unreleased areas to the released areas of the samples. Furthermore, then the material migrates preferable to the compliant, high curvature areas of the wrinkles.

The hypothesis that material migration already mainly takes place during the initial growth process is supported by the AFM topography images shown in figures 4(c) and (d). Figure 4(c) depicts the surface of the unreleased regime next to the frontier of a released area. The surface is comparable to the surface morphology seen after annealing (see figure 2(d)) and very close to the surface morphology of the initial processed surface (figure 1(d)). The height scale of 2.5 nm indicates that the surface is flat, but a small number of InAs island pre-cursors are visible in the AFM picture. Compared to the reference surface shown in figures 3(a) and (b), no major InAs island formation or accumulation can be observed. The AFM topography image depicted in figure 4(d) was obtained 12 μm away from the frontier between the released and unreleased areas. Even so, the surface morphology is still flat compared to the surface morphology observed for a reference sample [figure 3(b)], we can see a formation of small InAs island precursors. The overall height of 4.5 nm (the scale was deliberately reduced to 2.5 nm to allow comparison to image figure 4(c)) indicates that the small pre-islands are slightly larger. This result points to an island's formation tendency inside this sample region away from the released parts. As we do not detect full island formation at any position after post annealing, we conclude that this material migrates towards the wrinkled areas during our post-growth annealing. Furthermore, the low overall density of the islands proves that already during the growth process the InAs migrates to the released and wrinkled areas of the sample. Once reaching this area, the InAs stays there trapped and does not diffuse back to the unreleased parts of the sample resulting in the large material accumulation observed in the AFM images of figures 2(a), (b), and 4(a).

Material migration was also observed during the overgrowth of patterned samples [19]. This includes the formation of depletion regions around patterned area for island formation during InAs or Ge growth as well as preferred material accumulation at certain sample positions [9, 37]. These migration phenomena have been connected with diffusion-driven processes [9], but find their origin in a lateral modulation of the chemical potential. Thereby, material will migrate to the regions of a low chemical potential. Theoretical analysis of the chemical potential μ of the surface suggests a proportional connection between the surface potential and the misfit strain ϵ. The exact relation is still discussed [19, 38], but for our propose, we can assume $\mu \propto \epsilon$ [38] (instead of $\mu \propto \epsilon^2$ [19]).

To estimate ϵ in a semi-quantitative way and obtain an idea of the change of μ, we analyze the misfit strain of our samples. XRD results on released, wrinkled membranes show [29] that we observe three regions of different local lattice parameter: (i) unreleased areas; (ii) released, bond-back and therefore flat areas; and (iii) the wrinkles. As ϵ is related to the local lattice parameter of each of the regions, we will first estimate the local lattice parameter. This is straightforward for the regions (i) and (ii), where we can assume either the lattice parameter of the GaAs substrate a_{GaAs} [regime (i)] or a bulk lattice parameter of a fully relaxed $In_{0.33}Ga_{0.67}As$ layer a_{InGaAs} [regime (ii)]. For the wrinkled area [regime (iii)], we have to take into account the change of the surface lattice parameter due to the curvature κ of the surface, which strains the lattice. In the first approximation, we can assume that the surface strain $\epsilon_{surface}$ is given by $\epsilon_{surface} = \kappa \times z$, where z is the distance to the neutral plane assumed in the middle of the membrane (2.5 nm) [39]. From this, the local (in-plane) lattice parameter is given by $a_{surface} = a_{InGaAs} + a_{InGaAs} \times \epsilon_{surface}$.

To determine κ, we have to extract a representative height profile of the wrinkled membrane from our AFM images. An exemplary profile obtained from a wrinkle in figure 4(a) is depicted in figure 5(a), where all three regimes can be identified. On the right side of the scan the flat, unreleased layer is observed. Due to the removal of the underlying AlAs layer, a step marks the frontier between the relaxed and released regions, which finally exhibits a ca. 23 nm high wrinkle with a base of ca. 300 nm. We find a best fit of the wrinkle by an Gaussian function of the form $A \exp\{-(x)^2/(2w)^2\}$ (A being the height and w being the half-width of the fitted curve seen in the inset of figure 4(a); x denotes the position). Our best fit is partly in contrast to different works, which suggest a sinusoidal function for the wrinkles [39–41]. Using the fitted curve, we can estimate the lattice parameter for all regimes. The calculated lattice parameter is plotted in figure 5(b), with the $a_{GaAs} = 5.6535$ Å for the flat regime, a jump to $a_{InGaAs} = 5.784$ Å and finally with the local $a_{surface}$ for the wrinkled structure, which depends on the local κ. The abrupt change from a_{GaAs} to a_{InGaAs} results from our inability to estimate the lattice parameter for the step. But the AFM images clearly show that the membrane is continuous over the etching step. This was also seen in cross-section TEM images of released membrane structures [42]. Due to the curvature of the wrinkle, the lattice is locally compressed at the bottom of the wrinkle and strained at the top. A similar curvature has been calculated for bend-up membranes strained by InAs islands [15].

Finally, we can calculate ϵ using our lattice parameter plot. Unlike what is commonly done for MBE growth, we calculate the strain not relative to the substrate as this lattice parameter changes over the surface, but relative to the InAs bulk lattice parameter (6.05 Å). The lateral ϵ profile is plotted in figure 5(c) as the function of the position in the AFM height profile seen in figure 5(a). For the areas of the unreleased membrane, we obtain a compressive ϵ of 6.8% (typically for InAs to GaAs), whereas the compressive ϵ reduces for the released, bond-back flat areas to ca. 4.5%. Finally, the wrinkle exhibits a change in compressive ϵ with ca. 5% for the bottom of the wrinkle and $\epsilon = 1.7\%$ (compressive) for the top.

Our analysis reveals that we have a high ϵ and therefore a high μ on top of the unreleased membrane. In fact, we observe

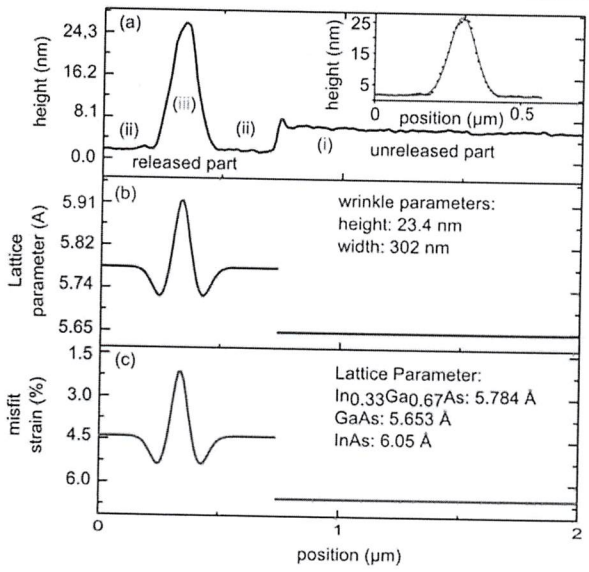

Figure 5. (a) Line scan obtained by AFM measures through the released and unreleased part. The three regimes with different lattice parameters are marked: (i) unreleased; (ii) released, back-bond (iii); released, wrinkled. (b) Calculated in-plane lattice parameter for the three sample regimes. (c) Calculated misfit strain in relation to the bulk InAs for the three regimes of the sample.

the formation of small InAs islands and bigger clusters during growth on our reference samples due to the large lattice mismatch. As soon as the material is offered a more attractive area on the sample, it diffuses already during growth to the released, wrinkled membrane as observed in figures 2(c) and 4(a). Finally, the curvature of the wrinkle explains why the material starts first to accumulate on the top of the wrinkle. Even if we assume an overestimation of the lattice parameter change due to κ, the analysis clearly reveals that the top of the wrinkles are areas with the lowest ϵ and therefore the lowest chemical potential μ.

Our analysis above addresses the thermodynamic aspects of the observed growth phenomena by analyzing the chemical surface potential. Besides the thermodynamic aspect, the kinetic aspect of the observed InAs migration has to be discussed. The InAs accumulation at the released, wrinkled areas indicates a directional diffusion for InAs deposited on unreleased parts of the samples. From our AFM image shown in figure 2(a), we concluded that the InAs migrates over distances as large as 60 μm completely to the released areas of the sample. Our observation of the formation of small pre-islands in figure 4(d) indicates that the indium migration occurs already during material deposition. Comparing our observed large migration length (of $\gtrsim$60 μm) with reported indium migration length for patterned GaAs substrates (8 μm) or flat GaAs surfaces (25 μm) [9, 43], we conclude that diffusivity must be higher on the unreleased parts of the sample compared to a GaAs surface. For a basic understanding, we have to take into account that the InAs is not deposited on a bare GaAs surface, but on an InGaAs surface compressively strained by 2.26%. In a simple model [44], the energy barrier for diffusion depends linearly on the strain of the underlying crystal. For Ge diffusing on compressive strain Ge (001), an increase of 100–1000 times has been reported [45]. Also, calculations for indium atoms on an InGaAs surface have been carried out [34], where the top InGaAs layer was a wetting layer for InAs island formation on GaAs (001). From these calculations [34], an increase of the indium diffusion coefficient from ca. 5e–6 $cm^2\,sec^{-1}$ on GaAs to 1e –3 $cm^2\,sec^{-1}$ on an InGaAs wetting layer on top of GaAs is predicated. Finally, an indium diffusion coefficient on an InAs wetting layer on top of GaAs (001) is calculated to 2e –4 $cm^2\,sec^{-1}$ (all values are for 750 K, close to our growth temperature). Hence, the indium diffusion is expected to largely enhance (100–1000 times), since it takes place on an InGaAs layer and indium adatoms on a compressively strained InGaAs surface are extremely mobile. Our results indicate that this predicated increased indium diffusivity is responsible for the material transport from the unreleased to the released areas of the samples over large distances. Indeed, if the more exact diffusion length value is desired, the patterned mesa size must be ~10 times enlarged (from 150 μm to 1.5 mm) in order to observe a clear gradient on the island density/volume.

Besides relaxed, back-bond areas, our samples exhibited sometimes small, freestanding areas (as pointed out during the discussion of figure 2(a)). The origin of such freestanding parts is ascribed to a similar mechanism observed in patterned Si-on-insulator samples [15]. Small pinholes allow the etchant to penetrate the top layer and give rise to—in our case due to the anisotropy of the HF etching to AlAs—rectangular freestanding, edge supported InGaAs membranes (a schematic cross-section is shown in figure 6(a)). Such freestanding membranes have demonstrated a great influence on the growth of self-assembled nanostructures, as they act as a compliant substrate accommodating some of the mismatch strain between the nanostructure and the substrate [15–17, 25, 26].

In figure 6(b), an AFM topographic image of such a freestanding area close to the edge of a sample with 0.5 ML of InAs deposition is shown. The freestanding area can be identified by its height contrast and the typical sharp edges arising from the anisotropic etching of the underlying AlAs sacrificial layer. The areas between the edge of the wrinkles and the freestanding parts are flat, exhibiting no island formation or material accumulation. Again, material accumulates not only on the wrinkles, but also on the freestanding parts competing with the wrinkled areas for the deposited InAs.

Figure 6(c) shows a detailed AFM image of the freestanding edge-supported membrane. In this image, a clear bending of the freestanding membrane is visible, either due to the strain relaxation after etching or due to the strain transfer of the deposited material [15, 17]. Furthermore, the topography already allows identifying the InAs islands formed on top of the membrane. A surface slope shown in figure 6(d) allows a clear identification of InAs islands or deposits. This plot reveals that the material tends to accumulate in the center of the freestanding membranes, whereas no material accumulation is observed on the frontier with the substrate. This is

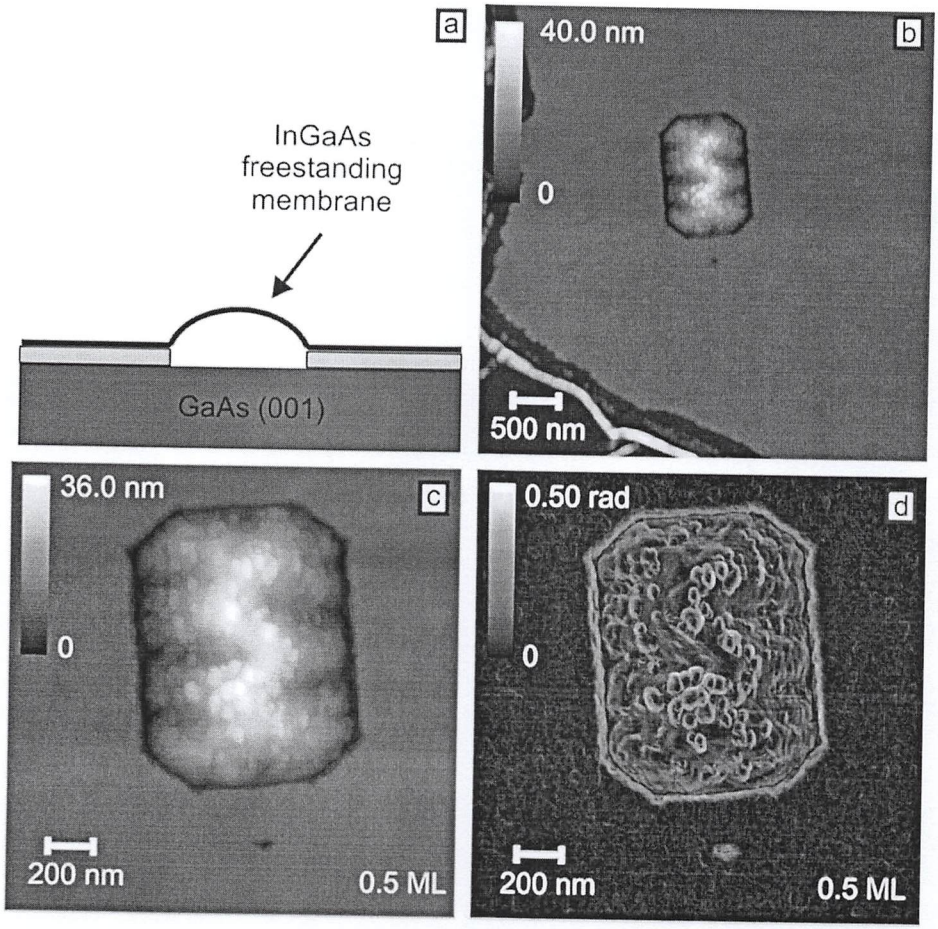

Figure 6. (a) Schematic illustration of the freestanding, edge-supported membrane. (b) Overview $5 \times 5\ \mu$m AFM image of the freestanding regime close to the edge between released and unreleased parts of the sample. (c) Topographic AFM image of freestanding membrane (d) surface slope image of the region calculated from image (a). The change in slope allows the identification of the islands.

in contrast to the observations for the back-bonded, relaxed membranes, where the frontiers between the relaxed and fixed parts were a good seeding area for InAs self-assembled nanostructures (see figure 4(a)). Similarly to the InAs islands formed on freestanding Si membranes [15], the islands tend to form in the middle of the membrane. Finite element analysis of such structures have shown [15] that this allows a better strain transfer from the island to the compliant substrate. Besides the better strain transfer, any pre-curvature of the membrane will drive the material to the middle of the membrane as the analysis of the local misfit for the wrinkled layer profiles reveals.

Finally, the question arises, if the large InAs accumulation on top of the membrane results in a breakdown of the pseudomorphic growth. To shed some light on this question, a sample with 2 ML InAs deposited was investigated with GIXRD.

A longitudinal scan around the GaAs (220) reflection of the sample is depicted in figure 7. We observe a peak at a scattering vector $q_{GaAs} = 3.142\ \text{Å}^{-1}$, which arises from the GaAs substrate indicating that our structures are still well

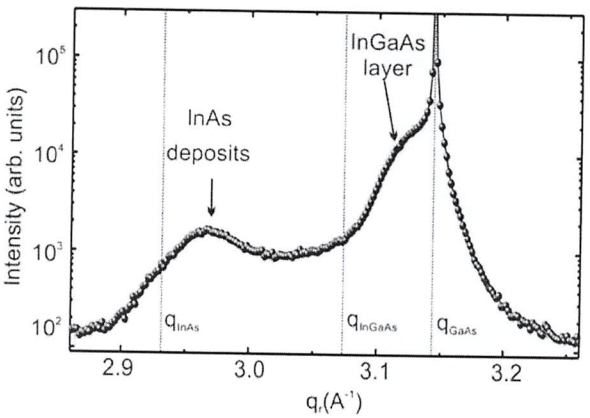

Figure 7. GIXRD longitudinal scan near the GaAs (220) reflection. The scan exhibits a peak of the GaAs substrate, an intensity gradient arising from the epitaxial, related to strain status originated from unreleased and partially released parts of the membrane and a broad peak ascribed to the deposited InAs material.

aligned to the substrate host lattice. Furthermore, an intensity gradient and broad peak spanning up to 2.90 $Å^{-1}$ are observed. Deposits with a lattice parameter close to InAs bulk ($q_{InAs} = 2.933$ $Å^{-1}$) can be the origin of the broad peak in the scan. We assign the shoulder near the GaAs peak to the unreleased pseudomorphically strained membrane, whereas the intensity gradient observed up to ca. 3.05 $Å^{-1}$ can be ascribed to different strain status at (partially) released positions of the InGaAs layer ($q_{InGaAs} = 3.073$ $Å^{-1}$ for fully relaxed $In_{0.33}Ga_{0.67}As$). Comparing this result to GIXRD of a released, wrinkled membrane [29], such distribution of lattice parameters with a long tail towards the GaAs bulk lattice parameter is expected. The existence of intermediate relaxation states in figure 7 indicate that parts of the deposited InAs are coherent to the substrate, while other regions undergo a plastic relaxation [46]. As our AFM results depicted in figures 2(a), (c) and 4(a) indicate that nearly all material migrates to the released areas of the sample, we assume that we overcome the critical thickness for relaxation on top of the membranes resulting in a formation of dislocations. A detailed structural investigation would be needed to identify the new critical thickness and growth behavior on the new virtual substrate presented by fully released membranes.

Conclusion

We investigated the overgrowth behavior of partly released, wrinkled InGaAs membrane structures for MBE deposited InAs. Round mesa structures are defined using lithography inside an $AlAs/In_{0.33}Ga_{0.67}As$ heterostructure. The top InGaAs layer is selectively under-etched to form a ca. 10 μm wide wrinkled, back-bonded area. Samples are chemically cleaned and introduced into an MBE, where an atomic hydrogen cleaning is carried out to remove the native oxide. Finally, different amounts of InAs are deposited on top of the samples and the material migration is studied using AFM. We find that the deposited InAs migrates over more than 60 μm and preferably accumulates on top of the released membrane, especially on top of the wrinkled structure. Quenching experiments carried out on samples immediately after growth indicate that most of the material migration takes place during the deposition process.

To obtain a semi-quantitative explanation for the origin of the migration process, we calculate the misfit strain relative to the deposited material for our structures. We obtain a low misfit strain due to the local curvature of the wrinkled membrane on top of the wrinkled. We concluded from these results that the material accumulates on these areas as the reduced misfit lowers locally the chemical potential. Similar material accumulations have been observed for patterned substrates [5, 19] and freestanding membranes [17, 18], which we also observe for the freestanding regimes of our samples. XRD results indicate a breakdown of the coherent growth, which we can ascribe to the large material migration and accumulation on top of the membrane.

Our first investigations show that the presence of different lattice parameters fundamentally changes the growth behavior of the well-investigated InAs/GaAs hetero-epitaxial system. Further detailed studies are needed to fully understand the growth dynamics on such samples, as well as to show how to obtain fully coherent structures. As the relaxation of the membrane lattice and the compliance of the thin freestanding membrane will change the critical thickness for deposition of lattice mismatched material and the strain inside the deposited heterostructure, such structures can act as virtual substrates allowing the tuning of optical and electrical properties of the deposited heterostructures.

Acknowledgements

The group of M Lagally (University of Wisconsin) is thanked for sharing their results with us and motivating the work. The constant help and interest of S O Ferreira (Universidade de Viçosa) is acknowledged. We thank the microfabrication (LMF) for access to the facilities and its staff (especially M H de Oliveira Piazzetta) for the support. The XRD of the sample was measured using the XRD2 beamline of the LNLS. Financial support was granted by FAPESP (Processo 2011/22945-1) and CNPq (Processo: 482729/2013-9). S.F C. acknowledges financial support by CAPES.

References

[1] Joyce B A and Vvedensky D D 2004 Self-organized growth on GaAs surfaces *Mater. Sci. Eng. R: Reports* **46** 127–76
[2] Cho A Y 1983 Growth of III–V semiconductors by molecular beam epitaxy and their properties *Thin Solid Films* **100** 291–317
[3] Cho A Y 1995 20 Years of molecular-beam epitaxy *J. Cryst. Growth* **150** 1–6
[4] Joyce B A and Joyce T B 2004 Basic studies of molecular beam epitaxy—past, present and some future directions *J. Cryst. Growth* **264** 605–19
[5] Kiravittaya S, Rastelli A and Schmidt O G 2009 Advanced quantum dot configurations *Rep. Prog. Phys.* **72** 046502
[6] Li X L, Wang C X and Yang G W 2014 Thermodynamic theory of growth of nanostructures *Prog. Mater. Sci.* **64** 121–99
[7] Bhattacharya P, Ghosh S and Stiff-Roberts A D 2004 Quantum dot opto-electronic devices *Annl. Rev. Mater. Res.* **34** 1–40
[8] Lan H and Ding Y 2012 Ordering, positioning and uniformity of quantum dot arrays *Nano Today* **7** 94–123
[9] Kiravittaya S, Rastelli A and Schmidt O G 2005 Self-assembled InAs quantum dots on patterned GaAs(001) substrates: formation and shape evolution *Appl. Phys. Lett.* **87** 243112
[10] Heidemeyer H, Müller C and Schmidt O G 2004 Highly ordered arrays of In(Ga)As quantum dots on patterned GaAs (001) substrates *J. Cryst. Growth* **261** 444–9
[11] Helfrich M, Schroth P, Grigoriev D, Lazarev S, Felici R, Slobodskyy T, Baumbach T and Schaadt D M 2012 Growth and characterization of site-selective quantum dots *Phys. St. Sol.* (a) **209** 2387–401
[12] Stangl J, Holý V and Bauer G 2004 Structural properties of self-organized semiconductor nanostructures *Rev. Mod. Phys.* **76** 725–83
[13] Atkinson P, Ward M B, Bremner S P, Anderson D, Farrow T, Jones G A C, Shields A J and Ritchie D A 2006 Site control

of InAs quantum dot nucleation by ex situ electron-beam lithographic patterning of GaAs substrates *Physica* E **32** 21–4

[14] Kohmoto S, Nakamura H, Nishikawa S and Asakawa K 2002 Three-dimensional site control of self-organized InAs quantum dots by in situ scanning tunneling probe-assisted nanolithography and molecular beam epitaxy *J. Vac. Sci. Tech. B: Microelectron. Nan. Struct.* **20** 762

[15] Deneke C, Malachias A, Rastelli A, Merces L, Huang M, Cavallo F, Schmidt O G and Lagally M G 2012 Straining nanomembranes via highly mismatched heteroepitaxial growth: InAs islands on compliant si substrates *ACS Nano* **6** 10287–95

[16] Ritz C S, Kim-Lee H-J, Detert D M, Kelly M M, Flack F S, Savage D E, Cai Z, Evans P G, Turner K T and Lagally M G 2010 Ordering of nanostressors on free-standing silicon nanomembranes and nanoribbons *New J. Phys.* **12** 103011

[17] Huang M, Rugheimer P, Lagally M G and Liu F 2005 Bending of nanoscale ultrathin substrates by growth of strained thin films and islands *Phys. Rev.* B **72** 085450

[18] Kim-Lee H J, Savage D E, Ritz C S, Lagally M G and Turner K T 2009 Control of three-dimensional island growth with mechanically responsive single-crystal nanomembrane substrates *Phys. Rev. Lett.* **102** 226103

[19] Yang B, Liu F and Lagally M G 2004 Local strain-mediated chemical potential control of quantum dot self-organization in heteroepitaxy *Phys. Rev. Lett.* **92** 025502

[20] Cavallo F and Lagally M G 2010 Semiconductors turn soft: inorganic nanomembranes *Soft Matter* **6** 439–55

[21] Rogers J A, Lagally M G and Nuzzo R G 2011 Synthesis, assembly and applications of semiconductor nanomembranes *Nature* **477** 45–53

[22] Scott S A and Lagally M G 2007 Elastically strain-sharing nanomembranes: flexible and transferable strained silicon and silicon-germanium alloys *J. Phys. D: Appl. Phys.* **40** R75–92

[23] Kim D H and Rogers J A 2008 Stretchable electronics: materials strategies and devices *Adv. Mater.* **20** 4887–92

[24] Huang M H, Cavallo F, Liu F and Lagally M G 2011 Nanomechanical architecture of semiconductor nanomembranes *Nanoscale* **3** 96–120

[25] Lo Y H 1991 New approach to grow pseudomorphic structures over the critical thickness *Appl. Phys. Lett.* **59** 2311

[26] Jones A M, Jewell J L, Mabon J C, Reuter E E, Bishop S G, Roh S D and Coleman J J 1999 Long-wavelength InGaAs quantum wells grown without strain-induced warping on InGaAs compliant membranes above a GaAs substrate *Appl. Phys. Lett.* **74** 1000

[27] Mei Y F, Thurmer D J, Cavallo F, Kiravittaya S and Schmidt O G 2007 Semiconductor sub-micro-/nanochannel networks by deterministic layer wrinkling *Adv. Mater.* **19** 2124

[28] Mei Y F, Kiravittaya S, Benyoucef M, Thurmer D J, Zander T, Deneke C, Cavallo F, Rastelli A and Schmidt O G 2007 Optical properties of a wrinkled nanomembrane with embedded quantum well *Nano Lett.* **7** 1676–9

[29] Malachias A, Mei Y F, Annabattula R K, Deneke C, Onck P R and Schmidt O G 2008 Wrinkled-up nanochannel networks: long-range ordering, scalability, and x-ray investigation *ACS Nano* **2** 1715–21

[30] Cendula P, Kiravittaya S, Mei Y F, Deneke C and Schmidt O G 2009 Bending and wrinkling as competing relaxation pathways for strained free-hanging films *Phys. Rev.* B **79** 085429

[31] Gill S P A 2011 An analytical model for the growth of quantum dots on ultrathin substrates *Appl. Phys. Lett.* **98** 161910

[32] Ni Y and He L H 2010 Spontaneous formation of vertically anticorrelated epitaxial islands on ultrathin substrates *Appl. Phys. Lett.* **97** 261911

[33] Sookchoo P, Sudradjat F F, Kiefer A M, Durmaz H, Paiella R and Lagally M G 2013 Strain engineered SiGe multiple-quantum-well nanomembranes for far-infrared intersubband device applications *ACS Nano* **7** 2326–34

[34] Rosini M, Kratzer P and Magri R 2009 In adatom diffusion on $In_xGa_{1-x}As$/GaAs(001): effects of strain, reconstruction and composition *J. Phys. Cond. Matter* **21** 355007

[35] Khatiri A, Krzyzewski T J, McConville C F and Jones T S 2005 Atomic hydrogen cleaning of low-index GaAs surfaces *J. Cryst. Growth* **282** 1–6

[36] Costantini G, Rastelli A, Manzano C, Songmuang R, Schmidt O G, Kern K and Känel H von 2004 Universal shapes of self-organized semiconductor quantum dots: striking similarities between InAs/GaAs(001) and Ge/Si (001) *Appl. Phys. Lett.* **85** 5673–5

[37] Kar G S, Kiravittaya S, Stoffel M and Schmidt O G 2004 Material distribution across the interface of random and ordered island arrays *Phys. Rev. Lett.* **93** 246103

[38] Shenoy V B, Tambe D T and Ramasubramaniam A *Comment on 'Local Strain-mediated chemical potential control of quantum-dot self-organization in heteroepitaxy'* (unpublished)

[39] Cendula P, Kiravittaya S and Schmidt O G 2012 Electronic and optical properties of quantum wells embedded in wrinkled nanomembranes *J. Appl. Phys.* **111** 043105

[40] Zhang Y, Yu M, Savage D E, Lagally M G, Blick R H and Liu F 2010 Effect of surface bonding on semiconductor nanoribbon wiggling structure *Appl. Phys. Lett.* **96** 111904

[41] Jiang H, Sun Y, Rogers J A and Huang Y 2007 Mechanics of precisely controlled thin film buckling on elastomeric substrate *Appl. Phys. Lett.* **90** 133119

[42] Deneke C, Jin-Phillipp N Y, Loa I and Schmidt O G 2004 Radial superlattices and single nanoreactors *Appl. Phys. Lett.* **84** 4475

[43] Arent D J, Nilsson S, Galeuchet Y D, Meier H P and Walter W 1989 Indium adatom migration during molecular beam epitaxial growth of strained InGaAs/GaAs single quantum wells *Appl. Phys. Lett.* **55** 2611–3

[44] Shu D, Liu F and Gong X 2001 Simple generic method for predicting the effect of strain on surface diffusion *Phys. Rev.* B **64** 245410

[45] Huang L, Liu F, Lu G-H and Gong X 2006 Surface mobility difference between Si and Ge and Its effect on growth of SiGe alloy films and islands *Phys. Rev. Lett.* **96** 016103

[46] Malachias A, Magalhães-Paniago R, Neves B R A, Rodrigues W N, Moreira M V B, Pfannes H-D, de Oliveira A G, Kycia S and Metzger T H 2001 Direct observation of the coexistence of coherent and incoherent InAs self-assembled dots by x-ray scattering *Appl. Phys. Lett.* **79** 4342

สำเนาถูกต้อง

Sumit Kiravittaya

สุวิทย์ กิระวิทยา